Article:
West, A.R., Jarkaneh, R., Dong, B. et al. (2016) Synthesis, structure and electrical properties of N-doped Li3VO4. Journal of Materials Chemistry A (4). pp. 1408-1413. ISSN: 2050-7488

https://doi.org/10.1039/C5TA07823G

Synthesis, Structure and Electrical Properties of N-doped Li_3VO_4

Bo Dong[1], Rouzbeh Jarkaneh[1], Stephen Hull[2], Nik Reeves-McLaren[1] and Anthony R West[1]

[1] University of Sheffield, Department of Material Science and Engineering, Mappin Street, Sheffield S1 3JD, U.K.

[2] The ISIS Facility, STFC, Rutherford-Appleton Laboratory, U.K.

Abstract

N-doped Li_3VO_4 of general formula $Li_{3+x}VO_{4-x}N_x$ was prepared by solid state reaction of Li_3N, V_2O_5 and either Li_2CO_3 or $LiOH{\cdot}H_2O$. A solid solution based on the low temperature β polymorph of Li_3VO_4 was obtained with composition $0 \leq x \leq 0.2$. Structural studies by x-ray and neutron powder diffraction confirmed the partial replacement of oxygen on the O(1) sites by N together with creation of an equal number of Li^+ ions which are located off-centre in adjacent octahedral Li(3) sites. Electrical property measurements on sintered pellets using impedance spectroscopy showed that the solid solutions are modest conductors of Li^+ ions, consistent with the partial occupancy of Li^+ ions in the interstitial octahedral sites. The activation energy for conduction of samples prepared using $LiOH{\cdot}H_2O$, ~ 1.91 eV, is much greater than for samples prepared, at higher temperature, using Li_2CO_3, ~ 0.78 eV and is attributed to ion trapping in $Li_i^{\cdot}$ / $N_0^{'}$ defect clusters. This study represents a relatively new method for doping Li^+ ions into a structure by anion doping which involves partial substitution of O by aliovalent N.

Introduction

With the increasing demand for high energy and power density lithium batteries for charge storage and electric vehicle applications, there is a need for new high-capacity electrode

materials, as well as high conductivity solid electrolytes for possible all-solid-state batteries[1]. Li_3VO_4 has been proposed as a possible anode material since it shows a reversible capacity of about 300mAhg^{-1} in the potential range from 0.2 to 3.0V. Its theoretical energy density is 2.5 times greater than that of $Li_4Ti_5O_{12}$ which is widely used as a lithium intercalation anode[2]. Li_3VO_4 has also been used as a surface coating on $LiCoO_2$ which is the cathode in many lithium ion batteries[3].

Li_3VO_4 shows temperature-dependent polymorphism with a low temperature β polymorph that is isostructural with β Li_3PO_4, an intermediate temperature, T polymorph whose structure is not known and a high temperature γ polymorph isostructural with γ Li_3PO_4[4]. At the highest temperatures, prior to melting, a fourth polymorph has been identified from thermal analysis but no structural information is available. The β and γ polymorphs belong to the family of tetrahedral structures; the β structures are ordered wurtzite superstructures derived from ZnO in which cations occupy one set of tetrahedral sites within a hexagonal close packed, HCP, oxide ion array[5]. The γ structures are related to the β structures but cations are now distributed over both sets of tetrahedral sites leading to edge-sharing of some tetrahedra. The oxide array is derived from HCP but the layers are more buckled than in the β structures. The oxide packing arrangement in the γ structures may also be regarded as tetragonal packed, TP, which in its ideal form is characterised by four fold symmetry, as in the case of rutile TiO_2.[6] The γ family of tetrahedral structures, including Li_3YO_4: Y = P, As, V, Cr and Li_2MXO_4: M = Mg, Zn; X = Si, Ge are the parent structures for a range of materials known as "lisicons" which have high Li^+ ion conductivity that are generated by forming solid solutions with phases Li_4ZO_4: Z = Si, Ge, Ti. More recently, there has been much interest in new cathode materials, Li_2MSiO_4: M = Mn, Fe in the same structural family since it is possible to de-intercalate Li^+ ions and activate redox couples associated with Mn and Fe[7]. There is also much recent interest in a new family of sulphur-based analogies of the lisicons known as thio-lisicons which are characterised by high levels of Li^+ ion conductivity at room temperature, giving possibilities of use as electrolytes in all-solid-state Li batteries[8].

Most studies on lisicon materials as either Li^+ ion conductors or as mixed conducting electrodes focus on compositional modification by cation doping within a fixed oxide ion sublattice. Our interest here is to investigate the possibility of anion, specifically N, doping, with creation of interstitial Li^+ ions for charge compensation. It follows on from work by the Oakridge group on LIPON materials which are nominally N-doped Li_3PO_4 but which are often glassy materials containing condensed phosphate anions rather than the isolated PO_4 tetrahedra of Li_3PO_4[9]. In this work we report a first study on the possible N doping of crystalline Li_3VO_4 and structural and electrical properties of the products. For the syntheses, two sources of Li were used: Li_2CO_3 and $LiOH{\cdot}H_2O$; $LiOH{\cdot}H_2O$ has the potential advantage that reaction occurs at significantly lower temperature than using Li_2CO_3.

Experimental

Reagents used were Li_3N, Li_2CO_3, $LiOH{\cdot}H_2O$ and V_2O_5. Li_2CO_3 and V_2O_5 were dried at 180°C before use; other reagents were used directly from the bottle. When using $LiOH.H_2O$, this was mixed with V_2O_5 in the required amounts and the mixture was heated at 150°C in N_2 to remove water. For the preparation of N-containing samples, the dried mixtures were returned to the glovebox to continue with the preparations. All weighing, mixing and pellet-pressing was carried out in the glovebox; weighed powders were mixed dry with an agate mortar and pestle and then pressed into pellets using a small hand press. Samples were reacted in molybdenum boats since there was some evidence of reaction with Li_3N if gold foil boats were used. Mixed powders were placed in the Mo boats which were inserted into glass tubes closed at one end. The other end was sealed with scotch tape and the tubes, with contents, were removed from the glovebox and placed in a horizontal tube furnace in flowing N_2. After purging the furnace atmosphere for 30 mins, the furnace temperature was increased at 5°C/min to either 650°C if Li_2CO_3 was used as the source of lithium or 450°C using $LiOH{\cdot}H_2O$ and held at that temperature for 10h. During heating, at ~ 150°C the scotch

tape cover of the glass tubes decomposed. At the end of the heat treatment, the furnace was cooled at 5°C/min, still under flowing N_2. In order to prepare samples for impedance measurements, pellets were reheated at 750°C for 10h under N_2. Samples for x-ray powder diffraction, XRD, were prepared in air and analysed using CuKα_1 radiation using a linear position sensitive detector on a ~~Stoe~~ STOE ~~Stadi~~ STADI P diffractometer. ~~Patterns were recorded over the 2θ range from 15° to 80° with a 0.02° scan rate.~~ For powder neutron diffraction, ND, the HRPD diffractometer at the Rutherford-Appleton Laboratory, U.K was used in time of flight, TOF, mode with incident wavelength in the range 0.5 to 12Å. Rietveld refinement was carried out using the EXPGUI interface of the GSAS suite of programmes.

For impedance measurements, pellets were coated on opposite faces with Au paste which was dried and hardened by heating at 800°C for 2h. Impedance data were collected with a Solartron analyser at 100*mV* ac over the frequency range 10^{-2} to 10^{6} Hz in N_2 atmosphere.

Comment [NRM1]: Need to add the reference for these:
A.C. Larson and R.B. Von Dreele, "General Structure Analysis System (GSAS)", Los Alamos National Laboratory Report LAUR 86-748 (2000).
B. H. Toby, *EXPGUI*, a graphical user interface for *GSAS*, *J. Appl. Cryst.* **34**, 210-213 (2001)

Results and Discussion

Samples of Li_3VO_4 and N-doped solid solutions of formula $Li_{3+x}VO_{4-x}N_x$: $0 \le x \le 0.2$ appeared to be single phase by XRD after synthesis at either 450°C using $LiOH{\cdot}H_2O$ or 650°C using Li_2CO_3 as shown in Fig. 1. Patterns were fully indexed on the unit cell of β Li_3VO_4 with slightly smaller lattice parameters for N-doped Li_3VO_4. Compositions with higher nitrogen content contained small amounts of Li_2CO_3, Fig. 1. From these data, we estimate the solid solution limit to be ~ x = 0.2. Similar results were obtained using either $LiOH{\cdot}H_2O$ or Li_2CO_3 as the source of Li_2O but reaction was achieved at significantly lower temperatures using $LiOH{\cdot}H_2O$, primarily because of the thermal stability of Li_2CO_3.

Structure refinement on two compositions x = 0 and x = 0.2 prepared using Li_2CO_3 was carried out using a combination of XRD and ND data. Initially, the thermal parameter, or U_{iso}, ~~of~~for ~~all~~ each atom~~s~~ was set to a default value~~s~~ (0.025 $Å^2$ for V and 0.01 $Å^2$ for other atoms). The background (6 terms of shifted Chebyshev function), scale factor and lattice

Formatted: Font: Italic
Formatted: Subscript
Formatted: Superscript

parameters were refined first followed by zero point and peak profile coefficient which were fixed after convergence. Then, the atomic coordinates of V were refined using XRD data and those of other atoms using ND data; these were fixed after convergence. Finally, the thermal parameters of all atoms were refined. The starting model was the reported structure of β Li_3VO_4 with space group $Pmn2_1$. Results for stoichiometric Li_3VO_4, x = 0, Table 1, were similar to those reported in the literature[10] and gave reasonable U_{iso} values for all positions with full site occupancy.

For the refinement of composition x = 0.2, scale factor, cell parameter, zero point, instrumental parameters and atomic parameters were refined in turn. It was assumed initially that the sample contained no nitrogen or interstitial lithium ions; occupancies of oxygen sites were refined giving a value for site O(1) significantly greater than unity, which was a strong indicator that oxygen may be partially replaced by nitrogen on that site since nitrogen is a stronger scatterer of neutrons than is oxygen. At this stage, $\chi^2 = 5.248$, $R_{wRp} = 9.54\%$ for ND and 3.38% for XRD, the occupancy of site O(1) was therefore refined allowing mixed occupancy by oxygen and nitrogen within a constraint of full occupancy, giving occupancy values of 0.12(2) for N and 0.88(2) for O with improved statistical parameters: $\chi 2 = 4.933$, ~~wRp~~$R_{wp} = 9.50\%$ for ND. The occupancies of sites O(2) and O(3) remained as unity within errors and therefore, there is no indication of significant nitrogen occupancy on these sites. In order to look for the presence of interstitial lithium ions, Fourier difference maps were constructed and a site Li(3) identified, Table 1. Its occupancy was set to 0.2, consistent with the value x = 0.2 in the starting composition and the value of the nitrogen content determined from the O(1) site occupancy and remained at 0.19(2) on refinement. The atomic coordinates of Li(3) were refined followed by occupancy of Li(3) to give a value of 0.19(3) when convergence was reached ($\chi^2 = 4.916$, $R_{wRp} = 9.48\%$ for ND). Then, U_{iso}s of all atoms except Li(3) were refined ($\chi^2 = 4.618$, ~~w~~$R_{wp} = 7.95\%$ for ND and 3.56% for XRD). In the final refinement, using combined ND and XRD data, the occupancies of O(1), N(1), Li(3) and the atomic coordinates of O(1), N(1), O(2), O(3), V, Li(1) and Li(2) were refined with fixed Uiso

Formatted: Superscript
Formatted: Subscript
Formatted: Font: (Default) Arial
Formatted: Superscript
Formatted: Subscript
Formatted: Font: Italic
Formatted: Subscript
Formatted: Superscript
Formatted: Subscript

values (χ^2 = 4.210, ~~w~~R_{wp} = 7.95% for ND and 3.25% for XRD). A subsequent refinement check of the U_{iso} values with fixed atomic coordinates and occupancies gave either small positive values or values of 0 within 2 esds for all atoms. Final refined parameters are listed in Table 1 for compositions x = 0 and 0.2, together with selected bond lengths and bond angles.

The partial substitution of N for O on the O(1) sites has little effect on the overall atomic coordinates of the crystal structure of x = 0.2 compared with x = 0. The new site for Li(3) is a distorted octahedral site with 3 short Li-O bonds typical of usual Li-O bond distances and 3 longer bonds in the range 2.56 to 2.70 Å, Fig 3. In the β structure of Li_3VO_4, one set of tetrahedral sites, T^+, pointing "up" in figure 3(a), are occupied whereas those pointing "down", T^-, are empty. The off-centre displacement of Li(3) in octahedral sites, (b), reduces the repulsions from cations in the adjacent occupied T^+ tetrahedral sites since the Li(3) ions are displaced towards the empty T^- tetrahedral sites.

The preference of N to substitute for O on the O(1) sites may be understood by considering the coordination environments of the three oxygen sites, Table 2. Bond lengths to the four tetrahedrally-coordinated atoms V, Li(1), Li(1)' and Li(2) are comparable for all three O sites and the difference is therefore associated with the possible coordination to Li(3). The O(1) site is coordinated to Li(3) with a reasonable Li – O, N bond length of 1.965 Å. However the corresponding O(2) bond to Li(3) length is significantly greater, 2.062 Å and O(3) is not coordinated at a reasonably short distance to Li(3). Given the higher nominal charge on nitrogen, 3^-, compared with that on oxygen, 2^-, the extra positive charge associated with Li(3) is balanced by substitution of N on adjacent O(1) sites. Consequently, coupled substitution of N on O(1) sites with an equivalent occupancy of adjacent Li(3) sites occurs leading to defect association.

A typical impedance dataset for N-doped Li_3VO_4 is shown in Fig. 4. Data are presented in four different complementary formats. In (a), impedance complex plane plots show a high frequency arc, which passes through the origin and a low frequency spike which becomes

Formatted: Superscript
Formatted: Subscript
Formatted: Font: Italic
Formatted: Subscript

an arc at high temperatures. Using the same data, plots of capacitance, C' against frequency, (b), show a high frequency plateau with value ~ 1-2pFcm^{-1} which is a typical value for a bulk capacitance with an associated permittivity in the range 10 – 20. At lower frequencies, the C' data increase to values as high as 10μF at a frequency of 10^{-2} Hz; such a high capacitance is indicative of electrode double layer phenomena, such as would be associated with ionic conduction of, in this case, Li^+ ions. Plots of log conductance, Y' against log f, (c), show a frequency independent plateau over a wide frequency range; at lower frequencies a dispersion to much lower conductivities occurs and is associated with the charge blocking at the sample-electrode interface. At high frequencies, a second dispersion to higher conductivity values is observed and is attributable to Jonscher power law behaviour of the sample bulk conductivity. Combined spectroscopic plots of Z''/M'', (d), show overlapping peaks at high frequencies which are attributable to the sample bulk response and the tail of a large peak at low frequencies in the Z'' spectrum associated with the blocking electrodes. The conclusion from these results is that the sample is electrically homogeneous with no evidence of a significant grain boundary impedance and that the sample is an ionic conductor whose bulk conductivity is given either from the intercept on the Z' axis (a) or from the frequency-independent Y' plateau in (c).

For undoped Li_3VO_4, the impedance data are similar to those for N-doped Li_3VO_4 but with the main difference being that the low frequency electrode spike is much less pronounced. Overall conductivity values are also 1-2 orders of magnitude lower. Pure Li_3VO_4 is expected to be an ionic and electronic insulator and the measured conductivity may therefore be attributed to either residual Li^+ conduction associated with slight departure from stoichiometry or the presence of, as-yet unidentified, electronic impurities.

Bulk conductivity data are presented in Arrhenius format in Fig 5 for both undoped and doped Li_3VO_4, prepared using the two different sources of Li_2O. In both cases, the conductivity of Li_3VO_4 increased by 1-2 orders of magnitude on doping with N and the creation of interstitial Li^+ ions. However the conductivities of both undoped and doped Li_3VO_4

are somewhat higher for materials prepared using $LiOH \cdot H_2O$; this is attributed to the presence of unidentified electronic impurities in the $LiOH \cdot H_2O$ starting materials. An additional difference between the two set of N-doped Li_3VO_4 samples is the activation energy for Li^+ ion conduction, which is much greater for samples prepared using $LiOH \cdot H_2O$. We attribute this to the strong defect association, involving Li(3) and N, leading to a higher activation energy for Li^+ ion conduction, in materials prepared using $LiOH \cdot H_2O$. Possibly this is because the higher synthesis temperature which was necessary using Li_2CO_3, led to reduced defect association and therefore, easier Li^+ ion conduction. If we assume that the activation energy of 0.78 eV for the sample prepared using Li_2CO_3 represents the activation energy for Li^+ ion migration, then that for the sample prepared using $LiOH \cdot H_2O$, 1.74 eV, contains an additional 0.96 eV that may represent the dissociation energy of Li(3)-N defect complexes.

The impedance data clearly show an increase in Li^+ ion conductivity on doping Li_3VO_4 with N. This correlates well with the crystallographic data which, for composition $Li_{3.2}VO_{3.8}N_{0.2}$, show the presence of an additional 0.2 Li^+ ions on the Li(3) site and the substitution of 0.2 N atoms on the O(1) site, in accord with the expected composition and assuming that no loss of Li and/or N occurs during synthesis.

The mechanism of Li^+ ion migration may involve direct interstitial migration between adjacent Li(3) sites, either in the ac plane or in adjacent ac planes, or an interstitialcy (or knock-on) mechanism involving the displacement of Li(1) or Li(2) ions from their regular lattice sites. In the ac plane, adjacent Li(3) sites are separated by empty tetrahedral, T_- sites, through which a migrating Li^+ ion must pass. These T_- sites share faces with occupied LiO_4 or VO_4 tetrahedra and strong cationic repulsions would prevent simultaneous occupation of adjacent T_- and T_+ sites, especially if one of these contains vanadium. The T_- sites, therefore, represent a saddle position in the Li^+ ion migration pathway between adjacent Li(3) sites. Alternatively, an interstitialcy or knock-on mechanism may operate which requires the ejection of a Li^+ ion from its occupied T_+ site which is then occupied by the incoming Li^+ ion.

In the b direction, direct interstitial migration between, face-sharing octahedral sites appears to be possible, as one step in the migration pathway between Li(3) sites in adjacent ac planes. We conclude that 3D conduction of Li^+ ions in N-doped Li_3VO_4 should be feasible although there may be a certain degree of anisotropy between conduction in the b direction and within the ac plane. It could be useful to probe the details of the migration mechanism and pathway by modelling studies.

Conclusions

Many examples of Li^+ conductivity in "lisicon" materials are known but, to date, these all involve solid solutions based on the parent γ polymorph of end-member phases, such as Li_3PO_4 and Li_2ZnGeO_4, and contain either Li^+ vacancies or interstitial Li^+ ions that are generated by aliovalent cation doping. The present study concerns the β polymorph of Li_3VO_4 and is the first example of a Li^+ ion conducting solid solution based on a β tetrahedral structure.

Combined ND/XRD studies confirm the substitution of O by N together with the creation of an equal number of interstitial Li^+ ions; defect pairs form by electrostatic attraction between N located on O(1) sites and occupied adjacent Li(3) interstitial sites. The composition determined by refinement of XRD/ND data matches that expected from the target stoichiometry and indicates the usefulness of the synthetic procedure developed for N-doping.

Impedance data show enhanced Li+ ion conductivity in the N-doped materials. Variation in activation energy between different samples may indicate whether or not the Li(3) ions are trapped by adjacent nitrogen atoms. Although anion doping, by N, represents a relatively untried method of modifying the Li content of a structure, trapping of interstitial Li^+ ions within defect complexes, and the associated increase in activation energy for conduction, may limit the usefulness of this method for generating a high level of Li^+ ion conductivity. Further studies on the general applicability of this doping method are planned.

References

(1) Fergus, J. W. J. of Power Source. 2010, 195, 4554.

(2) Li, H. Q.; Liu, X. Z.; Zhai, T. Y.; Li D.; Zhou, H. S. Adv. Energy Mater. 2013, 3, 428.

(3) Pu X.; Yu, C. G. Nanoscale. 2012, 4, 6743.

(4) West, A. R.; Glasser, F.P. J. Solid State Chem. 1972, 4, 20.

(5) West, A. R. Z. Krist. 1975, 141, 1.

(6) West, A. R.; Bruce, P. G. Acta Crys. 1982, 38, 1891.

(7) Dominko, R. J. of Power Source. 2008, 184, 462.

(8) Knauth, P. Solid State Ionics. 2009, 180, 911.

(9) Bates, J. B.; Dudney, N. J.; Gruzalski, G. R.; Zuhr, R. A.; Choudhury, A.; Luck, C. F. Solid State Ionics. 1992, 53-56, 647.

(10) Shannon, R. D.; Calvo, C. J. Solid State Chem. 1973, 6, 538.

Caption

Figure 1 X-ray diffraction patterns of $Li_{3+x}VO_{4-x}N_x$: x= 0, 0.2, 0.4. Samples used Li_2CO_3 as source of Li and were reacted at 750 ^oC for 10 h in N_2.

Figure 2 Observed, calculated and difference profiles from refinement of (a, b) Li_3VO_4 and (c, d) $Li_{3.2}VO_{3.8}N_{0.2}$ using XRD and ND data. Inserts in (b) and (d) show expanded d-space region from 2.2 to 2.6 Å.

Figure 3 Polyhedral structure of $Li_{3.2}VO_{3.8}N_{0.2}$. Blue and yellow tetrahedra are $Li(1,2)O_4$ and VO_4 respectively; green spheres are Li(3) in off-centre octahedral sites. Purple and red spheres are O, N(1) and O(2, 3) respectively.

Figure 4 Impedance data for $Li_{3.2}VO_{3.8}N_{0.2}$, prepared using Li_2CO_3. (a) Impedance complex plane plots at 332, 387, 449 ^oC. Spectroscopic plots of C' (b), Y' (c), –Z'' and M'' (d). Inset in (a) shows impedance data prepared using $LiOH{\cdot}H_2O$.

Figure 5 Arrhenius plots of $Li_{3+x}VO_{4-x}N_x$: x= 0, 0.2; Sample prepared using (a) Li_2CO_3, (b) $LiOH{\cdot}H_2O$. Activation energies are noted beside each data set.

Table 1(a) Refined structural parameters. (b) Bond lengths (c) Angles.

Table 2 Bond lengths to O(1), O(2) and O(3).

Figure 1

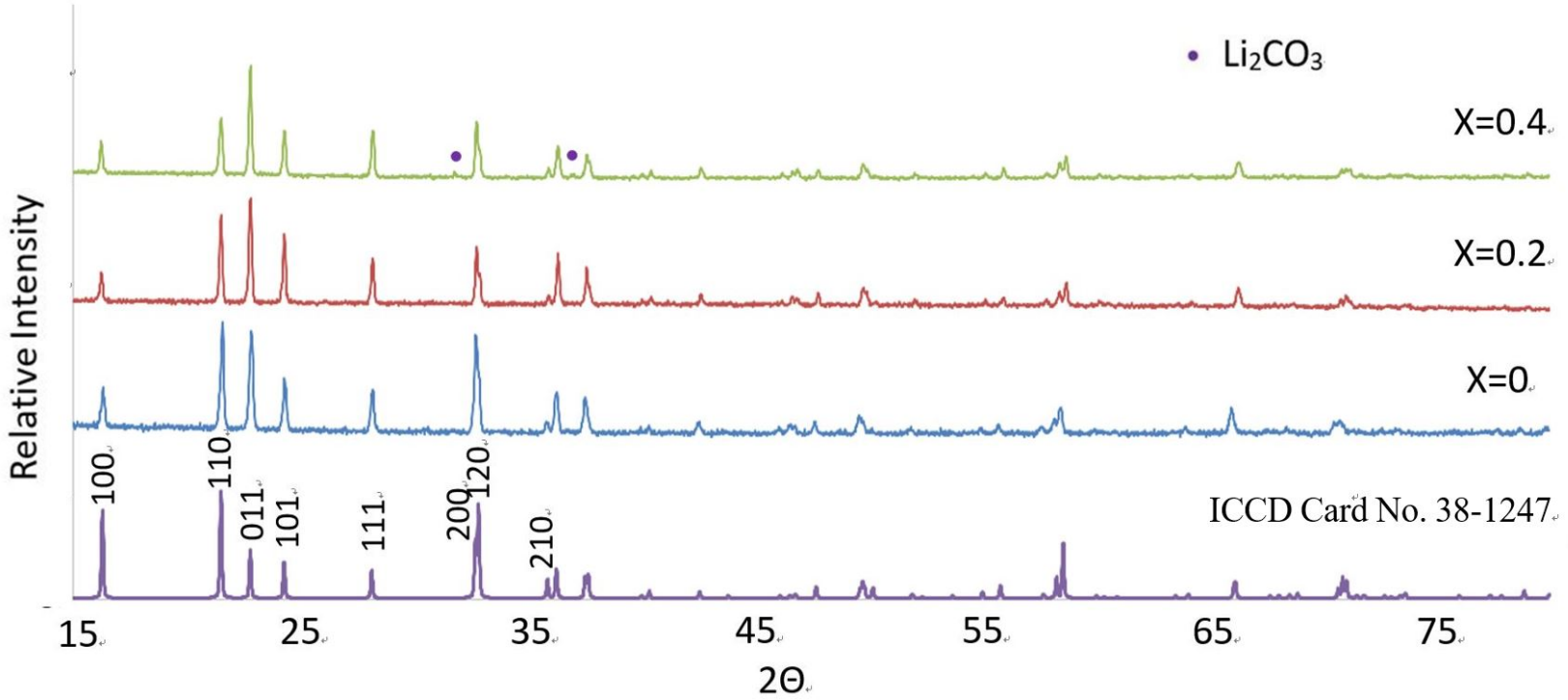
Li2CO3
X=0.4
X=0.2
X=0
Relative Intensity
100
110
011
101
111
200
120
210
ICCD Card No. 38-1247
15
25
35
45
55
65
75
2Θ

Figure 2

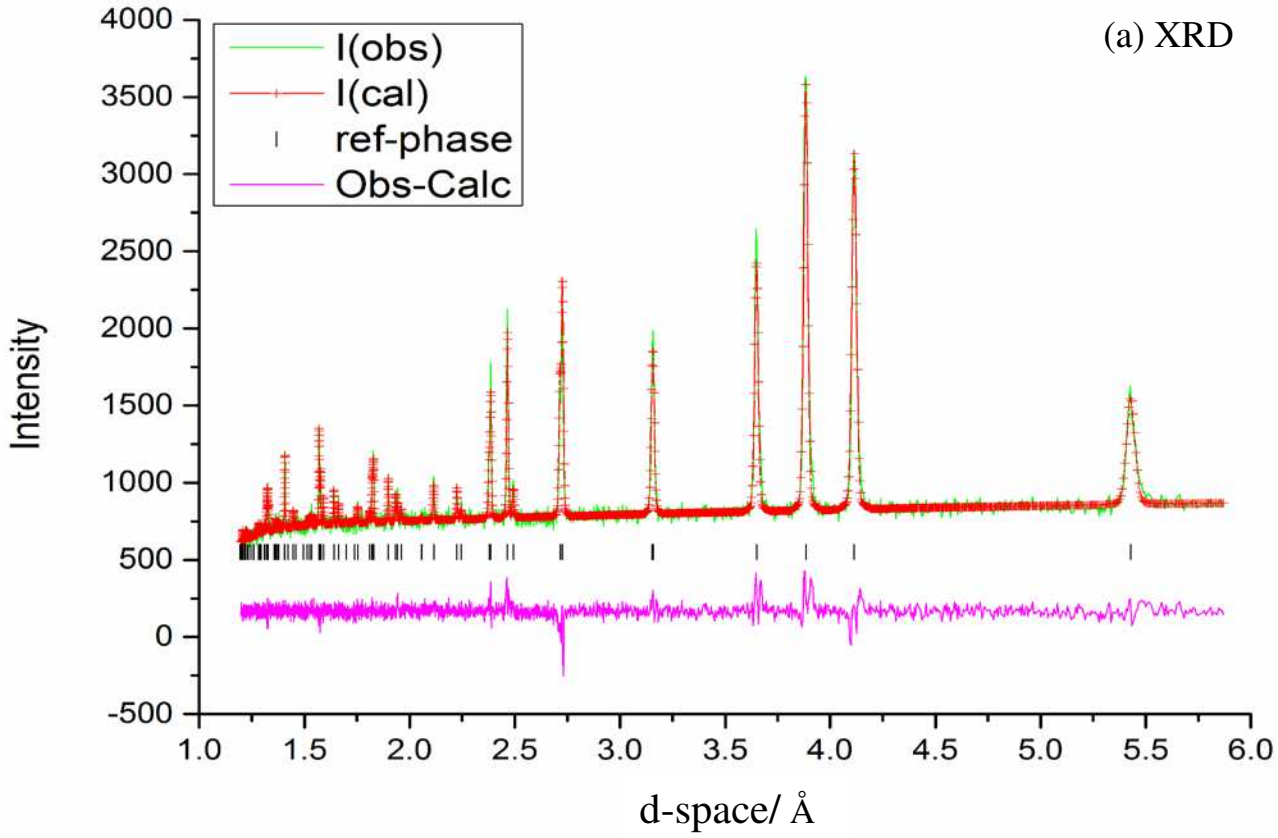
(a) XRD
I(obs)
I(cal)
ref-phase
Obs-Calc
Intensity
4000
3500
3000
2500
2000
1500
1000
500
0
-500
1.0
1.5
2.0
2.5
3.0
3.5
4.0
4.5
5.0
5.5
6.0
d-space/ Å

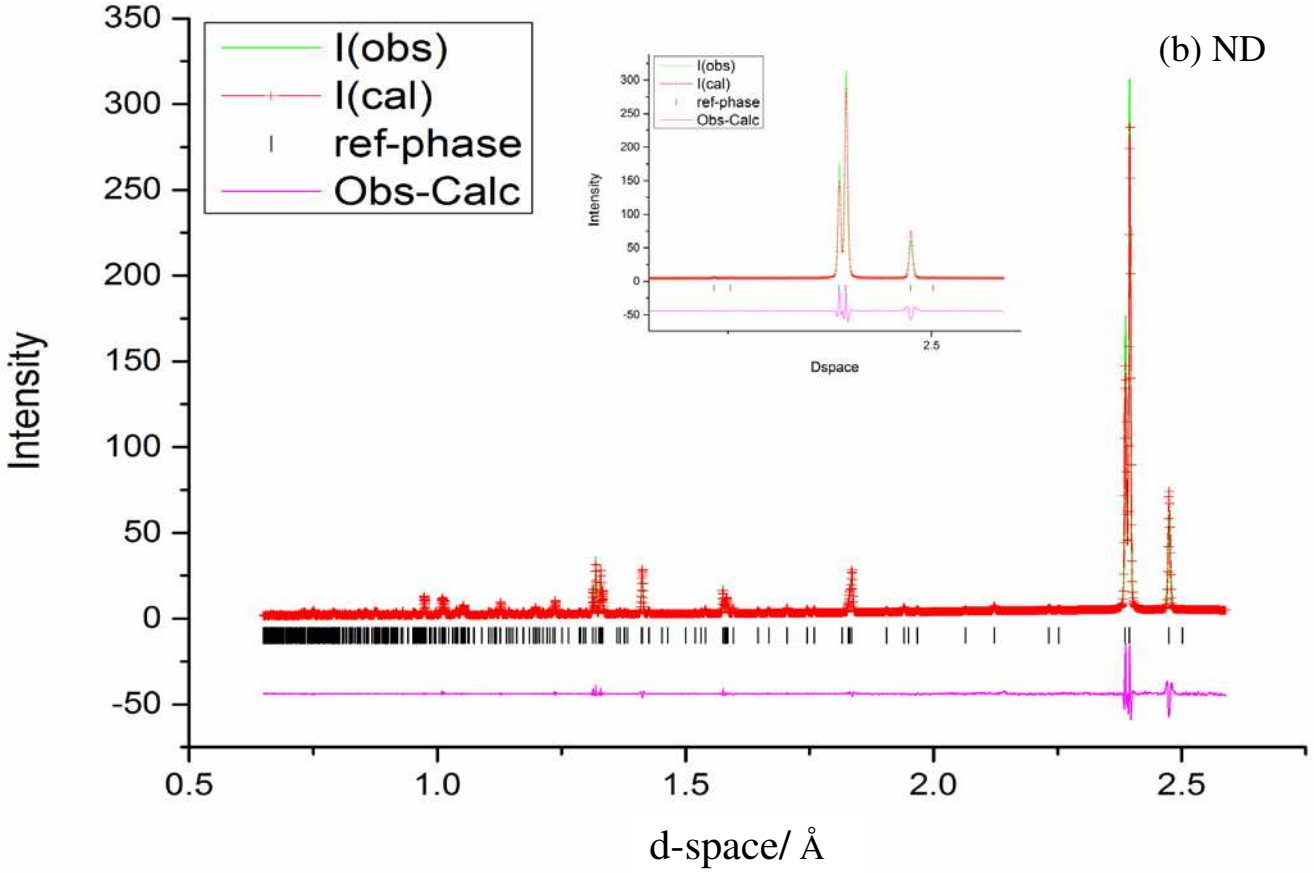

(b) ND

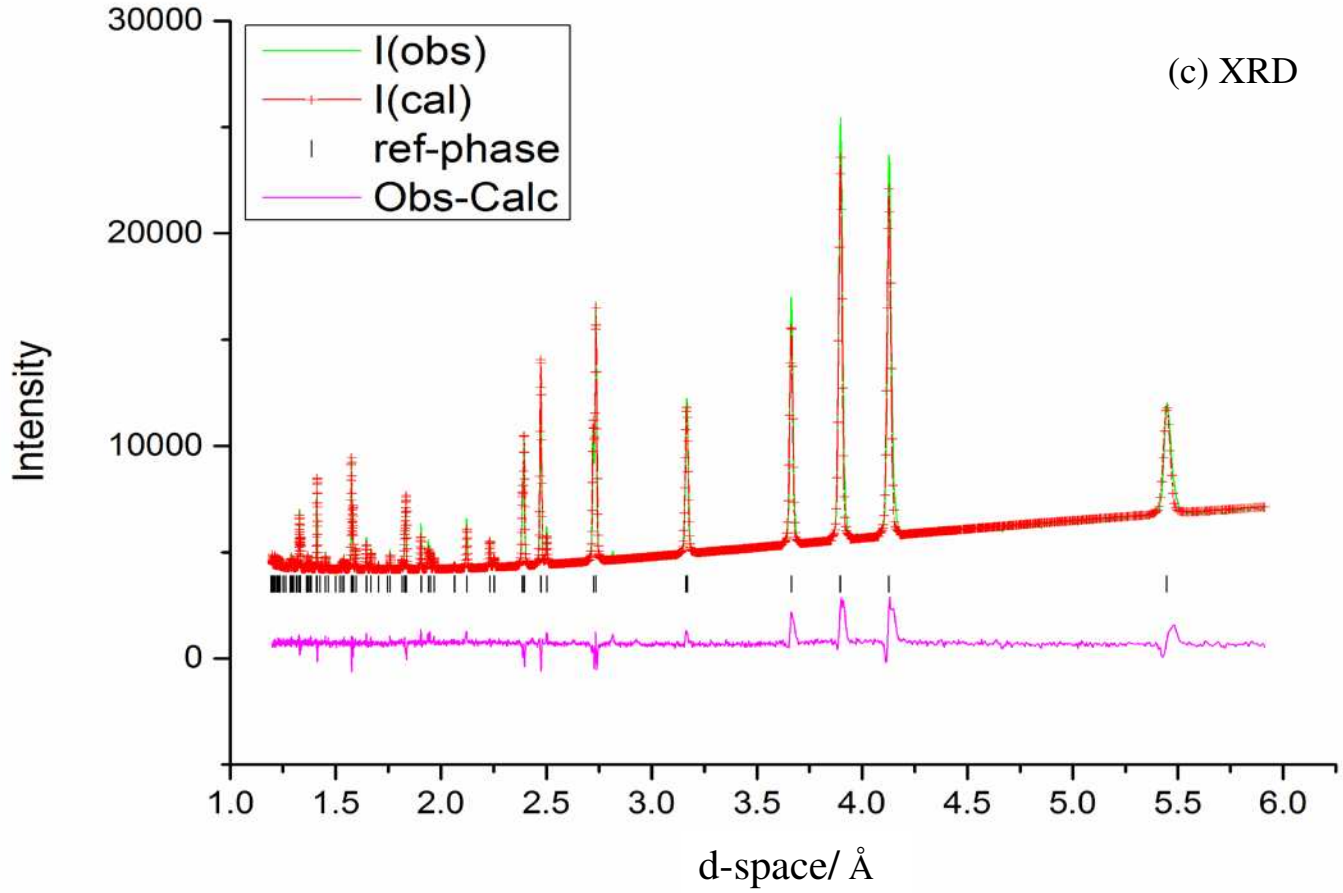
I(obs)
I(cal)
ref-phase
Obs-Calc
Intensity
30000
20000
10000
0
1.0
1.5
2.0
2.5
3.0
3.5
4.0
4.5
5.0
5.5
6.0
d-space/ Å

(c) XRD

(d) ND

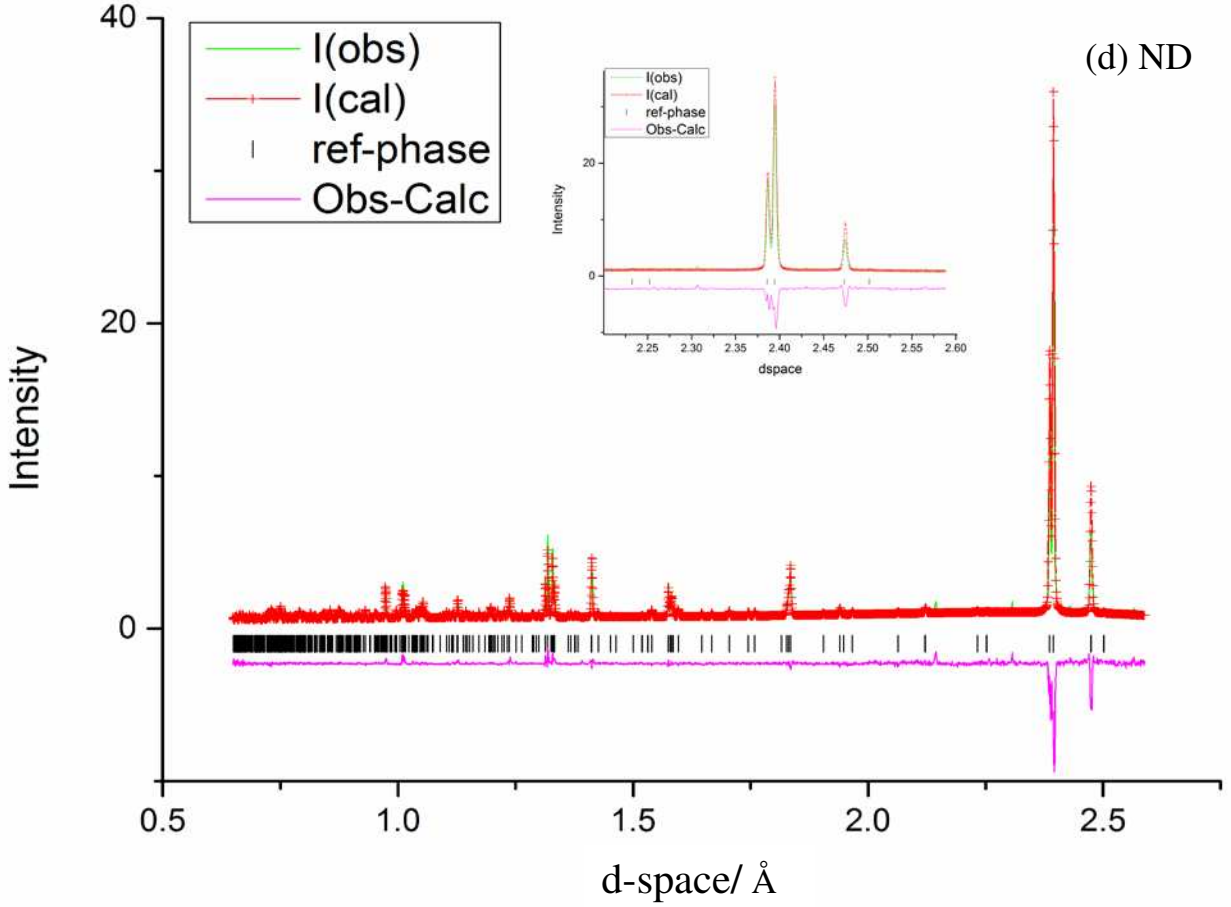
I(obs)
I(cal)
ref-phase
Obs-Calc
Intensity
d-space/ Å
40
20
0
0.5
1.0
1.5
2.0
2.5
dspace
2.25
2.30
2.35
2.40
2.45
2.50
2.55
2.60

Figure 3

(a)

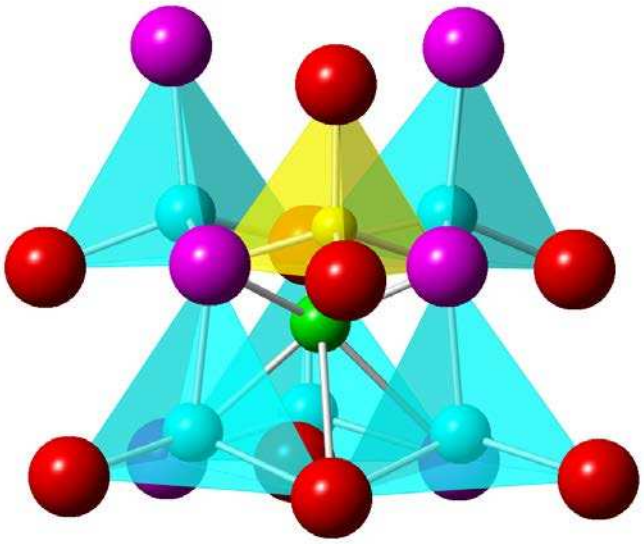

(b)

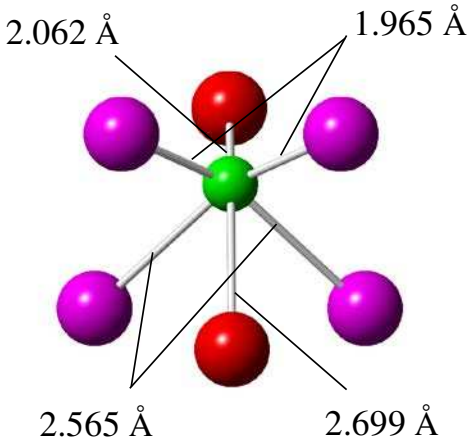

Figure 4

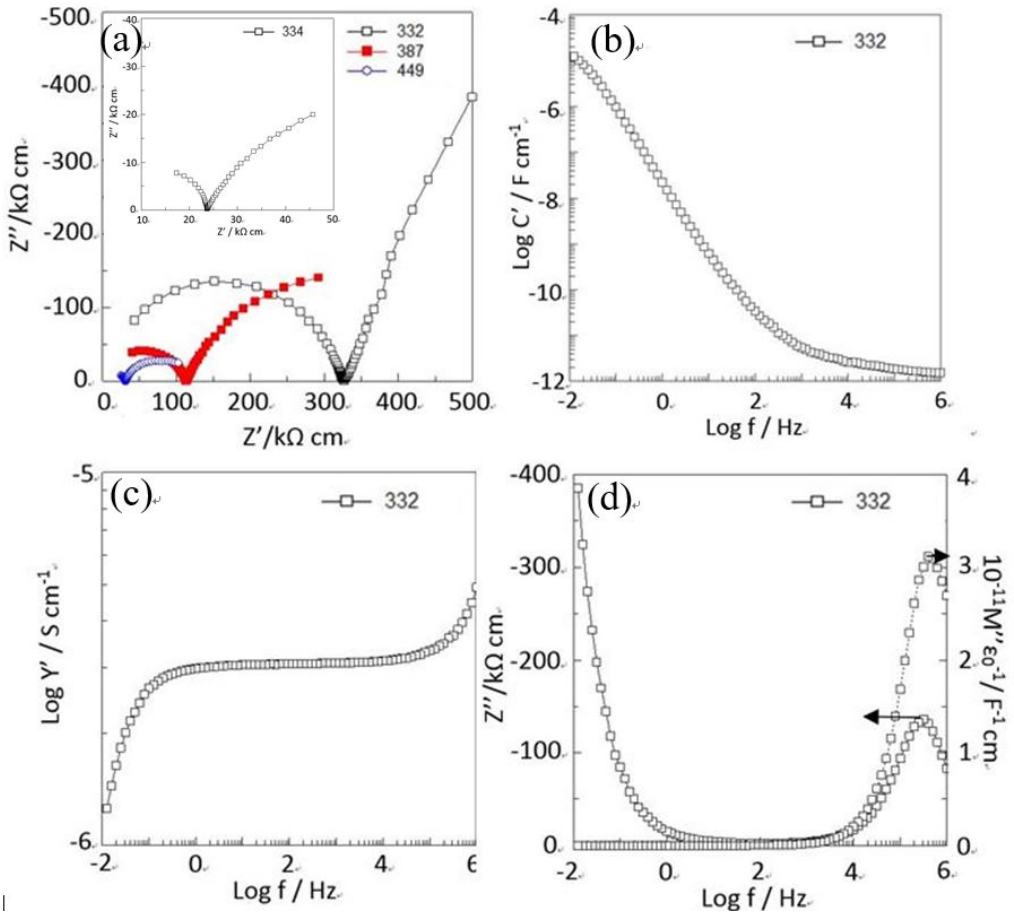
(a)
334
332
387
449
Z''/kΩ cm
Z'/kΩ cm
(b)
332
Log C' / F cm-1
Log f / Hz
(c)
332
Log Y' / S cm-1
Log f / Hz
(d)
332
Z''/kΩ cm
10-11M''ε0-1/ F-1 cm
Log f / Hz

Figure 5

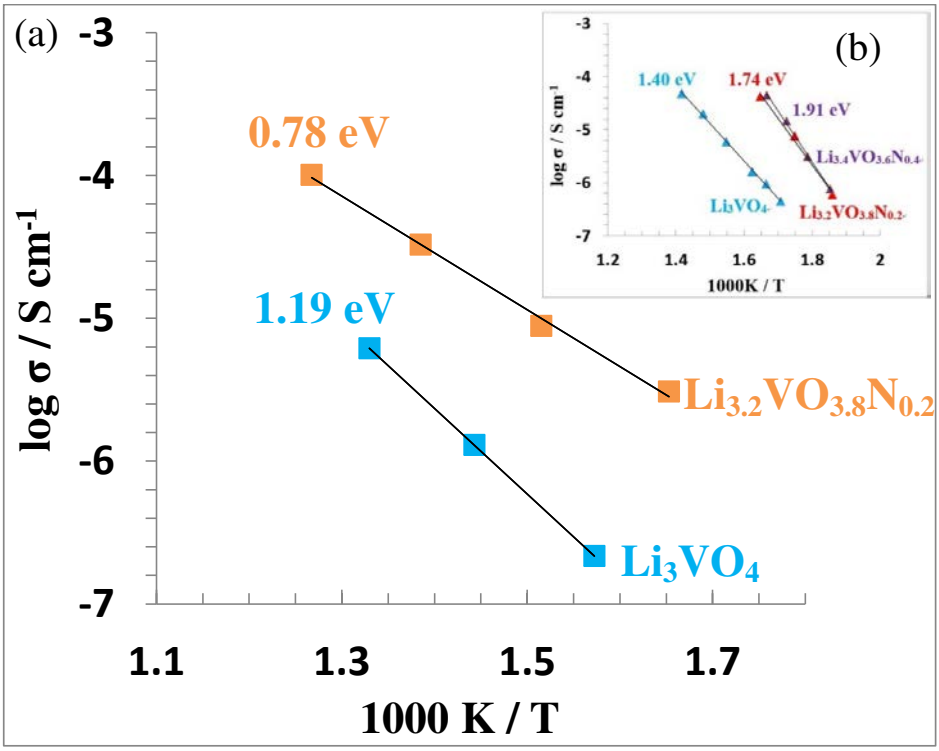
(a)
-3
-4
-5
-6
-7
log σ / S cm-1
0.78 eV
1.19 eV
Li3.2VO3.8N0.2
Li3VO4
1.1
1.3
1.5
1.7
1000 K / T
(b)
1.40 eV
1.74 eV
1.91 eV
Li3.4VO3.6N0.4
Li3VO4
Li3.2VO3.8N0.2
1.2
1.4
1.6
1.8
2
1000K / T

Table 1(a)

Atom and multiplicity	Parameter	Li_3VO_4 (x=0)	$Li_{3.2}VO_{3.8}N_{0.2}$ (x=0.2)
Li(1), 4	x	0.246(1)	0.247(1)
	y	0.331(1)	0.331(2)
	z	0.986(6)	0.991(2)
	Occupancy	1	1
	U_{iso} x 100 / Å^2	1.50(8)	0.24
Li(2), 2	x	0.5	0.5
	y	0.836(1)	0.832(3)
	z	0.985(6)	0.995(2)
	Occupancy	1	1
	U_{iso} x 100 / Å^2 ~~Uiso x 100 Å~~	1.8(1)	1.39
Li(3), 2	x	--	0.5
	y	--	0.523
	z	--	0.235
	Occupancy	--	0.19(3)
	U_{iso} x 100 / Å^2 ~~Uiso x 100 Å~~	--	1.0
V, 2	x	0	0
	y	0.828(1)	0.829(1)

Formatted: Font: Italic
Formatted: Subscript
Formatted: Superscript

	z	0	0
	Occupancy	1	1
	U_{iso} x 100 / Å^2 ~~Uiso x 100 Å~~	2.4(2)	2.67
O(1), 4*	x	0.224(1)	0.224(1)
	y	0.680(1)	0.679(1)
	z	0.888(6)	0.896(1)
	Occupancy	1	O1 0.88(2) N1 0.12(2)
	U_{iso} x 100 / Å^2 ~~Uiso x 100 Å~~	1.36(2)	0.01
O(2), 2	x	0	0
	y	0.123(1)	0.129(1)
	z	0.890(6)	0.899(1)
	Occupancy	1	1
	U_{iso} x 100 / Å^2 ~~Uiso x 100 Å~~	1.39(3)	0.13
O(3), 2	x	0.5	0.5
	y	0.174(1)	0.175(1)
	z	0.843(6)	0.847(1)
	Occupancy	1	1
	U_{iso} x 100 / Å^2 ~~Uiso x 100 Å~~	1.27(4)	0.34
a=6.3288(1) Å, b=5.4475(1) Å, c=4.9483(1) Å, V=170.602(4) Å3, χ2= 2.920, ~~w~~R_{wp}=5.90%, R_p=6.88% for ND, ~~w~~R_{wp}=4.59%, R_p=3.35% for			

Formatted: Subscript

Formatted: Subscript

Formatted: Subscript

Formatted: Subscript

XRD.
a=6.3271(1) Å, b=5.4470(1) Å, c=4.9478(1) Å, V=170.518 (2) $Å^3$, χ^2= 4.093, ~~wRp~~R_{wp}=7.88%, R_p=8.47% for ND, ~~wRp~~R_{wp}=3.21%, R_p=2.04% for XRD.

Formatted: Subscript
Formatted: Subscript
Formatted: Subscript
Formatted: Subscript

*For $Li_{3.2}VO_{3.8}N_{0.2}$, the O1 site contained a disordered mixture of 11% N and 89% O.

Table 1(b)

	Li_3VO_4	$Li_{3.2}VO_{3.8}N_{0.2}$
Vector	Length (Å)	Length (Å)
Li1-O1	1.968(5)	1.958(8)
Li1-O1	2.004(4)	2.013(7)
Li1-O2	1.961(4)	1.963(7)
Li1-O3	1.952(4)	1.952(7)
Li2-O1	2.000(3)	1.994(7)
Li2-O1	2.000(3)	1.994(7)
Li2-O2	2.013(6)	2.008(13)
Li2-O3	1.973(7)	2.007(13)
V1-O1	1.720(10)	1.713(2)
V1-O1	1.720(10)	1.713(2)
V1-O2	1.730(10)	1.712(4)
V1-O3	1.70(3)	1.717(4)
Li3-O1	--	1.965(3)
Li3-O1	--	1.965(3)

Li3-O2	--	2.062(2)
Li3-O1	--	2.565(2)
Li3-O1	--	2.565(3)
Li3-O3	--	2.699(4)

Table 1(c)

Angle	Degree(^{o})	Degree(^{o})
O1-Li1-O1	106.2(2)	105.8(4)
O1-Li1-O2	115.1(2)	115.6(4)
O1-Li1-O3	113.2(2)	113.2(4)
O1-Li1-O2	107.3(2)	106.8(4)
O1-Li1-O3	105.6(2)	105.9(3)
O2-Li1-O3	108.8(2)	108.8(4)
O1-Li2-O1	121.8(3)	122.1(7)
O1-Li2-O2	106.1(2)	106.9(4)
O1-Li2-O3	108.0(2)	107.3(4)
O1-Li2-O2	106.1(2)	106.9(4)
O1-Li2-O3	108.0(2)	107.3(4)
O2-Li2-O3	105.7(3)	105.4(6)
O1-V1-O1	110.9(1)	111.8(2)
O1-V1-O2	110.2(1)	111.4(1)
O1-V1-O3	108.5(1)	107.2(2)

O1-V1-O2	110.2(1)	111.4(1)
O1-V1-O3	108.5(1)	107.2(2)
O2-V1-O3	108.6(1)	107.5(3)
O1-Li3-O1	--	92.4(1)
O1-Li3-O2	--	110.89(1)
O1-Li3-O2	--	110.89(1)

Table 2

Bond Length(Å)	O(1)	O(2)	O(3)
V(1)	1.713(2)	1.712(4)	1.717(4)
Li(1)	1.958(8)	1.963(7)	1.952(7)
Li(1)’	2.013(7)	1.963(7)	1.952(7)
Li(2)	1.994(7)	2.008(13)	2.007(13)
Li(3)	1.965(3)	2.062(2)	--
Li(3)	2.565(2)	--	2.699(4)